

## OBSERVATIONS OF DOPPLER BOOSTING IN KEPLER LIGHT CURVES

MARTEN H. VAN KERKWIJK<sup>1,2</sup>, SAUL A. RAPPAPORT<sup>3</sup>, RENÉ P. BRETON<sup>1,2</sup>, STEPHEN JUSTHAM<sup>1</sup>, PHILIPP PODSIADLOWSKI<sup>4</sup>,  
ZHANWEN HAN<sup>5</sup>

*Submitted to ApJ*

### ABSTRACT

Among the initial results from *Kepler* were two striking light curves, for KOI 74 and KOI 81, in which the relative depths of the primary and secondary eclipses showed that the more compact, less luminous object was hotter than its stellar host. That result became particularly intriguing because a substellar mass had been derived for the secondary in KOI 74, which would make the high temperature challenging to explain; in KOI 81, the mass range for the companion was also reported to be consistent with a substellar object. We re-analyze the *Kepler* data and demonstrate that both companions are likely to be white dwarfs. We also find that the photometric data for KOI 74 show a modulation in brightness as the more luminous star orbits, due to Doppler boosting. The magnitude of the effect is sufficiently large that we can use it to infer a radial velocity amplitude accurate to  $1 \text{ km s}^{-1}$ . As far as we are aware, this is the first time a radial-velocity curve has been measured photometrically. Combining our velocity amplitude with the inclination and primary mass derived from the eclipses and primary spectral type, we infer a secondary mass of  $0.22 \pm 0.03 M_{\odot}$ . We use our estimates to consider the likely evolutionary paths and mass-transfer episodes of these binary systems.

*Subject headings:* binaries: eclipsing — stars: evolution — stars: individual (KOI 74, KOI 81) — techniques: photometric — white dwarfs

### 1. INTRODUCTION

It has long been realized that precision photometry from space could allow detailed probes of stellar interiors through pulsations, and of planetary and stellar companions through transits, eclipses, and flux variations due to tides and irradiation. With the launch of *Kepler*, measurements with long-term precision of at least 1 part in  $10^5$  are now being collected for an unprecedented sample of stars (Caldwell et al. 2010; Koch et al. 2010).

Among *Kepler*'s initial discoveries are two “objects of interest,” KOI 74 and KOI 81, that have striking light curves, showing both primary and secondary eclipses (Rowe et al. 2010a, hereafter R10; where needed, we refer to the original version posted on arXiv as R10v1). In both systems, the relative eclipse depths show that the more compact, less luminous object is hotter than its stellar host. This result became puzzling as R10v1 derived a clearly substellar mass for the secondary in KOI 74; their mass range for the companion in KOI 81 was also consistent with a substellar object. If the smaller, hotter companions were indeed planets or brown dwarfs, then it would not be obvious how their properties could reasonably be explained.

In this work, we re-analyze the *Kepler* data for KOI 74 and KOI 81, and show that the photometric data for KOI 74 contain clear evidence for Doppler boosting with orbital phase, in addition to ellipsoidal light variations. We use this to make

what is, as far as we are aware, the first measurement of a radial-velocity amplitude from photometry. With our amplitude, it is clear that the companion is not substellar, but rather has a mass of  $\sim 0.2 M_{\odot}$ . For KOI 81, we find that the mass is likely similar. We demonstrate that all properties are consistent with the companions being low-mass white dwarfs (WDs), and discuss possible evolutionary histories for these systems.

### 2. THE LIGHT CURVES REVISITED

We retrieved the light curves of KOI 74 and KOI 81 from the archive, and show the raw aperture fluxes in Figure 1. For both sources, one sees the eclipses and transits superposed on roughly quadratic trends; in KOI 81, one also sees the pulsations reported by R10. We first review what one can infer from the transits and eclipses, and then discuss additional information seen at other phases.

#### 2.1. Constraints from the Transit and Eclipse Light Curves

The transit and eclipse light curves were fitted with detailed models by R10, and we use their ephemerides and inclinations (see Table 1). For our purposes below, however, it is useful also to have the ratio  $R_1/a$ , where  $R_1$  is the radius of the primary, and  $a$  the semi-major axis. This ratio is well constrained by the eclipse, depending on the eclipse duration  $t_e$  (at half maximum depth) and inclination  $i$  via  $\sin^2(\pi t_e/P) \sin^2 i = (R_1/a)^2 - \cos^2 i$  (Russell 1912). We measured  $t_e/P$  graphically and list the values, as well as the inferred ratios  $R_1/a$  in Table 1. Note that the derivation assumes that the stars are spherical; if they are rotating rapidly, then the constraint is mostly on the equatorial radius (see Section 2.6).

The measurement of  $R_1/a$ , combined with Kepler's law, constrains the mean density of the primary,  $\bar{\rho}_1 = (R_1/a)^{-3}(3\pi/GP^2[1+q])$ . For both KOI 74 and KOI 81, the mass ratios  $q = M_2/M_1$  are small, and, as discussed by R10, the densities inferred for  $q \ll 1$ , of  $\sim 0.45$  and  $0.17 \text{ g cm}^{-3}$ , respectively, are consistent with those expected for main-

<sup>1</sup> Kavli Institute for Astronomy and Astrophysics, Peking University, Beijing, China

<sup>2</sup> Department of Astronomy and Astrophysics, University of Toronto, 50 St. George Street, Toronto, ON M5S 3H4, Canada; mhyk@astro.utoronto.edu

<sup>3</sup> 37-602B, MIT Department of Physics and Kavli Institute for Astrophysics and Space Research, 70 Vassar St., Cambridge, MA 02139, USA

<sup>4</sup> Sub-department of Astrophysics, University of Oxford, Keble Road, Oxford OX1 3RH, UK

<sup>5</sup> National Astronomical Observatories / Yunnan Observatory and Key Laboratory of the Structure and Evolution of Celestial Objects, Chinese Academy of Sciences, Kunming, 650011, China

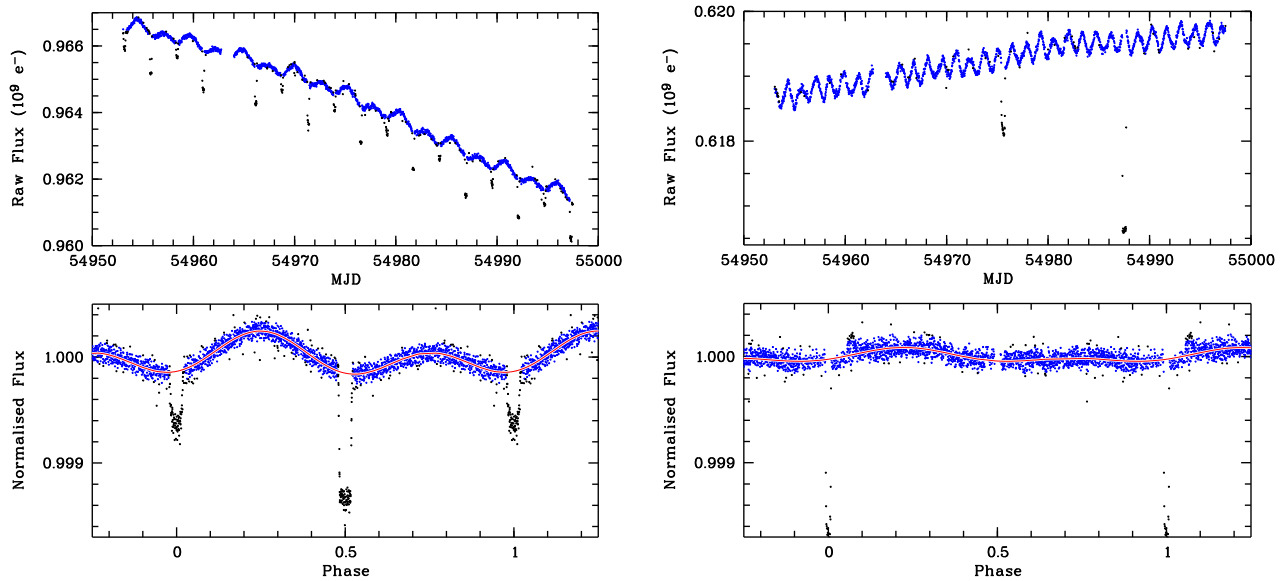


**Figure 1.** *Kepler* light curves for KOI 74 (left) and KOI 81 (right). The top panels show the raw photometric data, and the bottom panels the detrended and folded light curves. The larger dips correspond to eclipses of the hot companion, while the smaller ones correspond to transits over its parent star. The smooth curve represents a fit to the blue data points – those taken outside of transits and eclipses, and within  $3\sigma$ . The fit includes two sine waves, at the orbital and half-orbital period, representing Doppler boosting due to orbital motion and ellipsoidal light variations, respectively.

sequence stars with masses of  $2.2$  and  $2.7M_{\odot}$ , respectively, as inferred from their spectral types (see Table 1).

The ratio of the transit and eclipse depths  $\epsilon_t$  and  $\epsilon_e$  equals the ratio of the surface brightnesses. Thus, given the temperatures for the primaries inferred from their spectra, one can estimate the temperatures of the secondaries. Assuming blackbody emission, one has,

$$\frac{\epsilon_e}{\epsilon_t} \simeq \frac{e^{hc/\lambda kT_1} - 1}{e^{hc/\lambda kT_2} - 1}. \quad (1)$$

Using the numbers from Table 1 and assuming an effective wavelength  $\langle \lambda \rangle = 6000 \text{ \AA}$ , we infer  $T_2 = 13000$  and  $17000 \text{ K}$  for KOI 74 and KOI 81, respectively, with uncertainties somewhere between 5% and 10%. These temperatures are higher than inferred by R10, who assumed that the eclipses and transits measured bolometric surface brightness. (We note that, of course, one could derive more precise values by folding blackbodies or model atmospheres through the *Kepler* pass-band, but this would not necessarily be more accurate as long as one does not account properly for, e.g., gravity darkening on what may well be a rapidly rotating primary. In any case, for our purposes the above estimates suffice.)

## 2.2. Ellipsoidal Variations and Doppler boosting in KOI 74

For KOI 74, in addition to the long-term trend, eclipses, and transits, the raw fluxes show sinusoidal modulations at the orbital and half the orbital period (Figure 1). We fitted the data outside the eclipses and transits with a 6th-degree polynomial and sine waves at the orbital frequency and its harmonic (and iterated once, rejecting  $> 3\sigma$  outliers). In the bottom panel of the figure, where fluxes normalized by the polynomial component of the fit are shown as a function of phase, the modulations are very obvious. They have much larger amplitude than is seen in Fig. 1 of R10v1, likely because these authors originally had removed most of the signal in their pre-display median filtering; their later version shows a larger signal, more similar to what we find. (Related, we note that the two archive light curves include a ‘corrected’ flux. In the second, longer light curve, the signal is clearly present, but in the first, shorter

one, it is not, apparently having been removed by the ‘correction’ applied in the *Kepler* pipeline.)

From our fit, we infer fractional amplitudes  $\mathcal{A}_1 = (1.082 \pm 0.013) \times 10^{-4}$  and  $\mathcal{A}_2 = (1.426 \pm 0.018) \times 10^{-4}$  for the fundamental and the harmonic, respectively. As can be seen in Figure 1, these two fit the data quite well; although the fit is not formally acceptable ( $\chi_{\text{red}}^2 = 1.5$  for 1843 degrees of freedom), the residuals appear quite white. A Fourier transform of the residuals confirms this impression; there is no power above fractional amplitude  $10^{-5}$ , apart from one faint signal with  $\mathcal{A} \simeq 1.6 \times 10^{-5}$  and  $f \simeq 1.66 \text{ d}^{-1}$ . In Figure 1, one sees that the maximum of the fundamental coincides with one of the maxima of the harmonic; our fit gives a phase difference of  $-0.009 \pm 0.003$  cycles (of the orbital period; the maximum of the fundamental occurring slightly earlier). The fundamental has essentially the same offset ( $-0.008 \pm 0.002$  cycles) from the descending node of the massive star, while the harmonic has maxima coincident with the nodes to within the measurement errors ( $0.0005 \pm 0.0008$  cycles).

The above precisions are remarkable, and hence we checked whether the error estimates were reliable. We found that the amplitudes do depend on how we model the long-term trend; if we reduce the polynomial to 4th degree, we find  $\mathcal{A}_{1,2} = (1.034, 1.430) \times 10^{-4}$ ; if we fit the pipeline ‘corrected’ fluxes in the longer light curve with a constant and the two sine waves, we obtain  $\mathcal{A}_{1,2} = (1.076, 1.515) \times 10^{-4}$ . This suggests that the true uncertainty in the amplitudes is about 5%, although we note that these latter fits are not as good (we find  $\chi_{\text{red}}^2 = 1.7$ , and the phases do not agree as well with expectations). Obviously, the uncertainties will reduce substantially as further data are added.

Both signals have natural if, for the fundamental, unusual interpretations. We believe that the fundamental is due to orbital Doppler boosting, an effect which, as far as we are aware, was first detected and discussed by Maxted et al. (2000); it is discussed in the context of *Kepler* by Loeb & Gaudi (2003) and Zucker et al. (2007). Here, the precision of the *Kepler* data allows us to go beyond detection, and use the Doppler

boosting to measure a star's radial-velocity amplitude.

Briefly, Doppler boosting occurs because as the primary orbits, its spectrum is Doppler shifted, its photon emission rate is modulated, and its emission is slightly beamed forward. Following Loeb & Gaudi (2003), we use the relativistic invariant quantity  $L_\nu/\nu^3$  (or  $I_\lambda\lambda^5$ ), where  $L_\nu$  is the specific intensity, and  $\nu$  the frequency. Then, for a radial velocity  $v_r$ , the photon rate  $n_\gamma$  observed by a telescope with given effective area  $A_\lambda$  is given by,

$$n_\gamma = \int_\lambda A_\lambda \frac{F_\lambda}{hc/\lambda} d\lambda = \int_\lambda A_\lambda \frac{F_{\lambda'}(1+v_r/c)^{-5}}{hc/\lambda} d\lambda, \quad (2)$$

where  $F_\lambda \equiv \int_\Omega I_\lambda d\Omega$  is the observed flux ( $\Omega$  is the solid angle subtended by the star; note that the integral is correct only to first order in  $v_r/c$ ). For a narrow band, the fractional variation would then be

$$\frac{\Delta n_\gamma}{n_\gamma} \equiv f_{\text{DB}} \frac{v_r}{c} = \left( -5 - \frac{d \ln F_\lambda}{d \ln \lambda} \right) \frac{v_r}{c} \simeq - \frac{(hc/\lambda kT) e^{hc/\lambda kT} v_r}{e^{hc/\lambda kT} - 1} \frac{v_r}{c}, \quad (3)$$

where we introduced a Doppler boost pre-factor  $f_{\text{DB}}$  and where the approximate equality is for blackbody emission. For KOI 74 ( $T = 9400\text{K}$ ), observed with *Kepler* ( $\langle \lambda \rangle \simeq 6000\text{\AA}$ ), one thus expects a signal with fractional amplitude of  $\sim 2.8(K/c)$ , where  $K$  is the radial-velocity amplitude. For a more precise estimate, we folded a 9500K model atmosphere (Munari et al. 2005) through the *Kepler* response. This yields  $f_{\text{DB}} = 2.25$ ; the difference with the blackbody results from the fact that the model continuum is closer to Rayleigh Jeans inside the *Kepler* bandpass, mimicking the emission from a hotter blackbody. In this temperature range, the boost pre-factor scales approximately linearly with temperature; for  $T = 9000$  and  $10000\text{K}$ , we find  $f_{\text{DB}} = 2.37$  and  $2.15$ , respectively. Including reddening of  $E(B-V) = 0.15$  (from the *Kepler* Input Catalog) has only a small effect, yielding  $f_{\text{DB}} = 2.21$ . Given that adding the extinction is equivalent to a relatively large change in effective area, the small change in  $f_{\text{DB}}$  found also means that uncertainties in the response are not important.

Given the above, using  $f_{\text{DB}} = 2.21$ , our observed light amplitude corresponds to a radial-velocity amplitude of  $14.7 \pm 1.0\text{ km s}^{-1}$ , where we assumed 5% uncertainties in both  $\mathcal{A}_1$  and in  $f_{\text{DB}}$ . The corresponding mass function is  $\mathcal{M} = 0.0017 \pm 0.0004 M_\odot$ . If we adopt a mass for the primary star of  $2.22 M_\odot$  (R10; see Section 2.1), this yields  $M_2 \simeq 0.22 M_\odot$ .

Turning now to the harmonic, as in R10, we interpret it as changes in the observable surface area due to tidal distortion. The expected amplitude is given by,

$$\mathcal{A}_2 = f_{\text{EV}} \frac{M_2}{M_1} \left( \frac{R_1}{a} \right)^3 \sin^3 i, \quad (4)$$

where  $f_{\text{EV}}$  is a pre-factor of order unity that depends on the limb darkening and gravity darkening. For our system, the eclipse and transit light curves yield  $i$  and  $R_1/a$  (Section 2.1). Combining these with the amplitude yields a mass ratio  $M_2/M_1 = 0.092/f_{\text{EV}}$ . If we again adopt a primary mass of  $2.22 M_\odot$ , and take  $f_{\text{EV}} \simeq 1.5$  (see Section 2.5), we derive  $M_2 \simeq 0.14 M_\odot$ , somewhat below the value obtained above using the radial velocity amplitude, but roughly consistent, given the probably larger uncertainties associated with determining the mass ratio via ellipsoidal light variations (see Section 2.6).

### 2.3. Other Signals

Apart from the signals discussed above, one might also expect to see contributions of other factors, in particular the Doppler boosting and ellipsoidal variations of the secondary, irradiation effects on both primary and secondary, and possibly influences from an eccentric orbit. Following the procedure above, we find that the fractional amplitudes for the fundamental and harmonic of the secondary, relative to the secondary's flux, are  $\sim 10^{-3}$  and  $\sim 2 \times 10^{-7}$ , respectively (where we used  $K_2 \simeq 150\text{ km s}^{-1}$ ,  $f_{\text{DB}} = 1.9$ ,  $R_2/a \simeq 0.0026$ , and  $f_{\text{EV}} = 1$ ). Since the secondary's flux is only 0.2% of the total flux, however, the contribution to the observed signal is negligible.

For irradiation of the primary by the secondary, one expects a change in luminosity of  $\Delta L_1 \simeq \pi R_2^2 (L_2/4\pi a^2)$ , corresponding to a fractional amplitude  $\frac{1}{2} \Delta L_1/L = \frac{1}{2} (L_2/L) (R_2/2a)^2 \simeq 3.0 \times 10^{-6}$  (where  $L \simeq L_1$  is the total luminosity). Within the *Kepler* passband, this should lead to a modulation of  $\sim 1.7 \times 10^{-6}$ . Similarly, for the secondary, one expects a fractional amplitude of  $\frac{1}{2} (R_2/2a)^2 \simeq 0.8 \times 10^{-6}$  in bolometric flux, and a signal of  $\sim 0.4 \times 10^{-6}$  in the *Kepler* passband. The two will have opposite phase; thus, the net expected signal has an amplitude of  $\sim 1.3 \times 10^{-6}$ , and is phased such that maximum occurs at the time of transit. This signal may be responsible for the fact that the fundamental is slightly out of phase with what is expected from Doppler boosting; the observed out-of-phase amplitude is  $\mathcal{A}_1 \sin \Delta\phi_1 = (9 \pm 3) \times 10^{-7}$ , consistent with what we derived above.

Finally, we consider possible signals from a non-circular orbit. For small eccentricity, both the Doppler boost curve and the ellipsoidal variations would no longer be pure sinusoids, but have some contribution from higher harmonics. For the easier case of the Doppler boost curve, we can constrain the eccentricity from the absence of a signal at the first harmonic that is out of phase with that expected from ellipsoidal variations (to a limit of  $\Delta\phi_2 = 0.0005 \pm 0.0008$  cycles; Section 2.2). We find that, at 95% confidence,  $e \sin \omega = (\mathcal{A}_2/\mathcal{A}_1) \sin 4\pi \Delta\phi_2 < 0.03$  (where  $\omega$  is the longitude of periastron, and this expression is valid in the limit of small  $e$ ). One sees that one cannot constrain the case where periastron occurs at one of the nodes, since in that case the harmonic would be hidden by the ellipsoidal variations. A complementary constraint, however, comes from the fact that the mid-transit and mid-eclipse times are consistent with a circular orbit. The measured offset from half a cycle is  $\Delta\phi = 0.0003 \pm 0.0008$  cycles, which, at 95% confidence, implies  $e \cos \omega = \pi \Delta\phi < 0.006$  (with the expression again being valid in the limit of small  $e$ ). Thus, from both constraints combined, we conclude that the orbit is circular to within  $e < 0.03$ .

### 2.4. Application to KOI 81

For KOI 81, a detailed analysis is not possible, since variations on its much longer orbital period are strongly covariant with the trends in the raw data. Furthermore, the star is clearly pulsating; a Fourier transform shows that there is signal at numerous frequencies. In order to look for orbital modulation, we fit the raw fluxes with orbital and half-orbital modulations, a 3rd degree polynomial, as well as sine waves at the five largest pulsational signals, at 0.362, 0.723, 0.962, 1.32, and  $2.08\text{ d}^{-1}$  (some of these are harmonically related, as is often the case for multi-periodic pulsators). From the fit, orbital modulation does appear to be present, as is also clear in the

**Table 1**  
System parameters

Property	KOI 74		KOI 81	
	Primary	Secondary	Primary	Secondary
$P_{\text{orb}}$ (d)	5.18875 ± 0.00008		23.8776 ± 0.0020	
$i$ (°)	88.8 ± 0.5		88.2 ± 0.3	
Eclipse duration (cycle)	0.0362 ± 0.0004		0.058 ± 0.004	
Eclipse depth ( $10^{-5}$ )	51 ± 5	118 ± 5	160 ± 5	496 ± 5
$R/a$	0.116 ± 0.002	0.0026 ± 0.0002	0.058 ± 0.004	0.0023 ± 0.0003
Spectral type	A1 V	...	B9–A0 V	...
Radius ( $R_{\odot}$ )	1.90 <sup>+0.04</sup> <sub>-0.05</sub>	0.043 ± 0.004	2.93 ± 0.14	0.117 ± 0.012
$T_{\text{eff}}$ (K)	9400 ± 150	13000 ± 1000	10000 ± 150	17000 ± 1300
Luminosity ( $L_{\odot}$ )	25.6 ± 2.4	0.05 ± 0.02	77.3 ± 9.6	0.9 ± 0.4
Velocity amplitude ( $\text{km s}^{-1}$ )	14.7 ± 1.0	...	~7	...
Mass ( $M_{\odot}$ )	2.22 <sup>+0.10</sup> <sub>-0.14</sub>	0.22 ± 0.03	2.71 <sup>+0.19</sup> <sub>-0.11</sub>	~0.3
Model mass ( $M_{\odot}$ )	...	0.20 ± 0.03	...	0.25 ± 0.03

**Note.** — The periods and inclinations are taken from Rowe et al. (2010a), as are the spectral types of the primaries and the quantities inferred from those. Systematic errors are possible if the star has accreted significant matter, or is rotating rapidly. The eclipse durations and depths were measured graphically, and have “chi-by-eye” uncertainties. For the temperatures of the secondaries, we assumed an 8% systematic uncertainty in our conversion of surface brightness to temperature. The velocity amplitude is measured from the Doppler boost signal, and its uncertainty includes possible systematic effects related to the detrending of the data and the precise spectrum of the primary. The model mass is based on the theoretical relation between orbital period and WD mass (see Equation (5)).

folded, normalized light curve, where we divided the fluxes by the fitted trend and pulsational signals (see Figure 1). Our fit yields amplitudes  $\mathcal{A}_1 \simeq 5 \times 10^{-5}$  and  $\mathcal{A}_2 \simeq 4 \times 10^{-5}$ , which corresponds to  $K_1 \simeq 7 \text{ km s}^{-1}$  and  $q \simeq 0.2/f_{\text{EV}}$ . Because of the long orbital period, the results are very sensitive to, e.g., the degree of the polynomial used. Comparing with a fit using a 6th degree polynomial, as well as one using the ‘corrected’ flux from the *Kepler* archive light curve (the latter for the second, longer light curve only), the amplitude of the fundamental changes by up to a factor of 2, while that of the harmonic changes by  $\sim 20\%$ . Furthermore, we find relatively large phase offsets, of  $\sim 0.03$  cycles. Given this, we will not try to infer quantities, but simply note that for a  $2.7 M_{\odot}$  primary with a  $0.3 M_{\odot}$  companion, the predicted amplitudes are  $\sim 8 \times 10^{-5}$  and  $3 \times 10^{-5}$ , respectively, consistent with the observations.

### 2.5. Verification Using a Light Curve Synthesis Code

We tried to verify our semi-analytical estimates above using a light-curve synthesis code, which is similar to that of Orosz & Hauschildt (2000), and has been used previously to model irradiated pulsar companions (Stappers et al. 1999). The code accounts for tidal distortion and stellar rotation in the Roche approximation, includes irradiation and gravity darkening, and calculates the flux using NextGen model atmospheres (Hauschildt, Allard, & Baron 1999), integrated over the *Kepler* passband. It cannot yet deal with eclipses, and hence we only attempt to reproduce the orbital modulations.

As input parameters, we chose to use the set  $P_{\text{orb}}$ ,  $t_0$ ,  $i$ ,  $T_1$ ,  $R_1/a$ ,  $K_1$ ,  $P_{1,\text{rot}}$ ,  $q$ , and  $T_{\text{irr}}$ , where the ones not mentioned before are  $t_0$ , the time of conjunction, and  $T_{\text{irr}}$ , the effective temperature corresponding to the secondary flux absorbed by the primary (i.e.,  $\sigma T_{\text{irr}}^4 = (1-A)L_2/4\pi a^2$ , with the albedo  $A$  expected to be close to zero for a radiative star). Our main goal is to constrain  $q$ ,  $K$ , and  $T_{\text{irr}}$ ; we assume the other parameters are as inferred from the eclipses. For our fits, we also assume that the star is corotating with the orbit ( $P_{1,\text{rot}} = P_{\text{orb}}$ ); we will return to this in Section 2.6. We add to the model the tiny flux contribution from the secondary (taken to be constant at the level indicated by the eclipses).

Fitting the raw data of both sources to our model, we confirmed that for KOI 81, the results depend sensitively on how one fits the long-term trend. We thus decided to focus on KOI 74. We searched over a grid in  $q$ ,  $K_1$ , and  $T_{\text{irr}}$ , and fitted for the best 4th-degree polynomial at each position. The best-fit synthetic light curve is nearly indistinguishable from the two-sine fit, and has the parameters  $q = 0.0689 \pm 0.0009$ ,  $K = 14.2 \pm 0.2 \text{ km s}^{-1}$ , and  $T_{\text{irr}} = 760 \pm 40 \text{ K}$ . We did not exclude outliers, and therefore our fit is poorer than the analytical one ( $\chi_{\text{red}}^2 = 2.6$ ); we scaled the uncertainties such that  $\chi_{\text{red}}^2 = 1$  (but did not attempt to include uncertainties in effective temperature, etc.).

These results reproduce our analytical estimates. The offset in  $K_1$  would be even smaller if we had included reddening in our numerical model (as this affects  $f_{\text{DB}}$ ; see Section 2.2). The mass ratio matches our estimates for  $f_{\text{EV}} = 1.34$ , quite close to the value of  $f_{\text{EV}} = 1.63$  inferred from the tables of Beech (1989). The secondary luminosity inferred from the irradiation is  $0.08 \pm 0.02 L_{\odot}$  (for orbital separation  $a = 16.4 R_{\odot}$  and  $A = 0$ , i.e., assuming complete absorption and reradiation), consistent with our estimate from the surface brightness ratio. Below, we give our best estimates of the masses based on these results, but first we discuss possible uncertainties due to rapid rotation.

### 2.6. Uncertainties due to Rotation

In many ways, the light curves of KOI 74 and KOI 81 are easy to model, since all effects are small and can thus adequately be treated as perturbations. The one parameter that we have not yet constrained, however, is the rotation of the primary. Since rapid rotation is expected in the context of the evolutionary scenario described below, we discuss the observational consequences in some detail.

Rotation of the primary has a number of effects. First, the constraints on inclination and radius of the primary from the eclipse and transit change: the true inclination  $i'$  will be closer to  $90^\circ$  than the inclination  $i$  inferred assuming a spherical star, the radius will be smaller, and the radius that is constrained is the equatorial radius  $R_{\text{eq}}$  (assuming aligned rotation). Furthermore, the estimate of the mean density increases, to  $\bar{\rho}'_1 \simeq (R_{\text{eq}}/a)^{-3}(3\pi/GP^2[1+q])(R_{\text{eq}}/R_{\text{pole}})$ , where  $R_{\text{pole}}$  is the po-

lar radius; thus, one would infer a somewhat smaller primary mass. For KOI 74, which has an inclination very close to  $90^\circ$ , we conclude that it would have  $R_{\text{eq}}/a \simeq R_1/a$ . For KOI 81,  $R_{\text{eq}}/a$  would be somewhat smaller than  $R_1/a$  inferred from the eclipses.

The second effect of a rapidly rotating primary is that its pole will be hotter than the equator; hence, looking at the equator, one will underestimate its temperature, and thus its luminosity and mass. This also affects the estimates for the secondary, since the ratios of the radii ( $R_2/R_1$ ), based on the transit depth, and that of the surface brightnesses (Equation (1)) will be different from their true values: the cooler equator will lead to a larger inferred  $R_2/R_1$  and smaller inferred  $T_2$ . For the companion radius  $R_2$ , however, the change in  $R_2/R_1$  is partly compensated by the fact that a rapidly rotating primary also would have a smaller area ( $R_1' \simeq (R_{\text{eq}}R_{\text{pole}})^{1/2}$ ; see above). We have used our model code to test an illustrative case of extreme rotation, with the primary rotation rate 20 times faster than the orbital one (corresponding to  $v \sin i \simeq 370 \text{ km s}^{-1}$ ), and a ratio of equatorial to polar radius  $R_{\text{eq}}/R_{\text{pole}} = 1.32$  (similar to what is measured for Regulus; see McAlister et al. 2005). Keeping the flux-weighted temperature at 9400 K, we find equatorial and polar temperatures of  $\sim 7800$  and  $11600 \text{ K}$ , respectively. For this particular example, we estimate that the radius of the hot companion would be  $R_2' \simeq 0.045 R_\odot$ , i.e., increased by only 5% from that inferred for a slowly rotating primary, and its temperature  $T_2' \simeq 10500 \text{ K}$ .

Rapid rotation also indirectly affects the ellipsoidal variations. First, because of the different temperature distribution on a rapidly rotating primary, different regions are weighted differently, and as a result the amplitude of the ellipsoidal variations changes. From our model code, we find that for the above-mentioned case, the predicted amplitude of the ellipsoidal variations increases by a factor  $\sim 2$ . The effect is strongly non-linear, however; reducing the rotation rate from 20 to 15 times faster than orbital, the amplitude increases only by a factor of 1.3.

Another indirect effect of a rapidly rotating primary may be that the inferred  $q$  does not necessarily correspond to the true mass ratio. An implicit assumption underlying the equilibrium tide is that the primary corotates with the orbit. For stars that do not rotate synchronously, the work of, e.g., Pfahl, Arras, & Paxton (2008), suggests that the equilibrium tide may be a rather poor approximation to reality. Thus, it may be that one cannot reliably infer mass ratios from ellipsoidal variations for systems that are not tidally locked.

We note that the light curves may contain a clue to the rotation rates. In particular, for KOI 74, we found evidence for a weak modulation at  $\sim 0.6 \text{ d}$ , which is about 9 times faster than the orbital period, and corresponds to 30% of break-up for a  $2.2 M_\odot$  and  $1.9 R_\odot$  star. For KOI 81, it may be possible to infer the rotation rate from the pulsations by looking for rotational splitting (though for high rotation rates this is non-trivial).

Of course, it would be simpler and more reliable to measure the rotational broadening spectroscopically, and the spectra mentioned by R10 may already hold the answer, but we do not have access to those. Nevertheless, we note in closing a much more subtle consequence of rapid rotation, which is the photometric analog of the Rossiter-McLaughlin effect (Rossiter 1924; McLaughlin 1924). Assuming the rotation is aligned with the orbit, at the start of the transit more blueshifted light

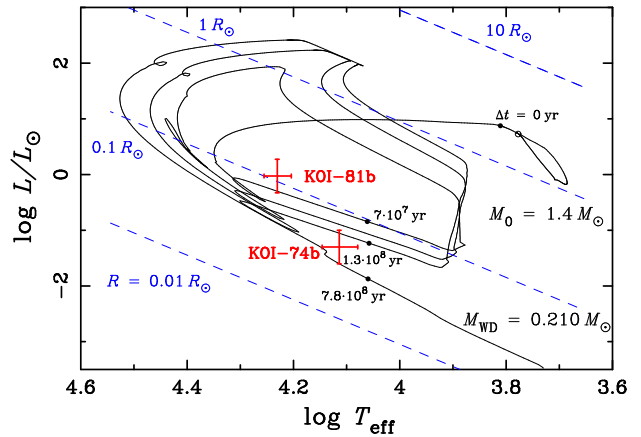


**Figure 2.** Representative evolutionary track in the Hertzsprung-Russell (HR) diagram, illustrating the evolution of the progenitors of the hot companions of KOI 74 and KOI 81. The solid black curve shows the track of a star with an initial mass of  $1.4 M_\odot$  that starts to transfer mass to a companion star just after leaving the main sequence and ultimately becomes a  $0.21 M_\odot$  helium WD. Because of residual hydrogen in the envelope at the end of the main mass-transfer phase, the degenerate remnant experiences three hydrogen shell flashes, producing three large loops in the HR diagram (of progressively larger area), before it settles on a classical He WD cooling track. Selected ages since the end of the main mass-transfer phase (labelled as “ $\Delta t = 0 \text{ yr}$ ”) are given next to filled circles. The dashed lines give lines of constant radius as indicated. The positions of KOI 74b and KOI 81b are also shown with conservative error bars. They are consistent with the expected location for  $\sim 0.2\text{--}0.25 M_\odot$  He WDs either on a classical He WD cooling track or during one of the relatively long-lived phases of a H-flash loop.

is being blocked and at the end more redshifted light. For a rotational velocity of  $300 \text{ km s}^{-1}$ , Doppler boosting induces a signal in the blocked light with a fractional amplitude of  $\sim 2 \times 10^{-3}$ . This is diluted by the unblocked light, i.e., by a factor equal to the transit depth. Thus, for KOI 74 and KOI 81, one expects net signals of  $\sim 1 \times 10^{-5}$  and  $3 \times 10^{-6}$ , respectively, which may be detectable by averaging about 100 transits.

## 2.7. Adopted Masses

In principle, given our inferred values of  $K_1$  and  $q$ , combined with the inclination, one can derive both masses without further assumptions. In practice, however, these masses are very uncertain, since the uncertainties in  $K_1$  and  $q$  enter to high powers (for small  $q$ ,  $M_1 \propto K_1^3 q^{-3}$  and  $M_2 \propto K_1^3 q^{-2}$ ). Given that these uncertainties are of order 5% for  $K_1$  and likely larger for  $q$  (see above), the  $1\sigma$  fractional errors are  $\gtrsim 20\%$ , and the distributions are highly non-Gaussian.

Instead, we proceeded by assuming the primary has a mass of  $2.22_{-0.14}^{+0.10} M_\odot$ , as inferred from its spectral type and mean density (R10; see also Section 2.1). Then, using  $K_1$  and  $i$ , we calculate a mass of  $0.22 \pm 0.03 M_\odot$  for the secondary. If instead we use the mass ratio  $q$ , inferred from the ellipsoidal variations, we find  $M_2 = 0.15 M_\odot$ , with an uncertainty that is difficult to estimate because we cannot be sure the star is in corotation (see above). We will proceed by using the value inferred from  $K_1$  (see Table 1). For KOI 81, we do not have a good constraint on  $K_1$  (or  $q$ ), but the signals that are present are consistent with a similar secondary mass, of  $\sim 0.3 M_\odot$ .

## 3. EVOLUTIONARY HISTORY

An obvious explanation for these hot, compact companions is that they are WD stars. R10 have discussed this possibility for KOI 81, but their initial very low mass estimate for the companion in KOI 74 ( $\leq 0.032 M_\odot$ ; R10v1) was inconsis-

tent with a WD explanation. Since our reanalysis of the data gives the mass of the companion in KOI 74 as  $\sim 0.2 M_{\odot}$ , a WD companion is no longer excluded. Cooling tracks from Panei et al. (2007) for helium-core WDs of appropriate mass are broadly consistent with the companion luminosities and temperatures in Table 1 (somewhat more easily for KOI 74 than for KOI 81). Figure 2 compares a cooling track from our own calculations<sup>6</sup> for a  $\sim 0.2 M_{\odot}$  helium-core WD to the WDs in KOI 74 and 81.

Binary systems resembling these may well be common; the well-known star Regulus ( $\alpha$  Leonis) has recently been found to be a spectroscopic binary with component masses  $\sim 0.3$  and  $3.4 M_{\odot}$ , and an orbital period of 40.11 d (Gies et al. 2008). The lower-mass component likely is a WD, making Regulus and its companion remarkably similar to the pair of systems considered here. The evolution of Regulus has been considered in detail by Rappaport, Podsiadlowski, & Horev (2009).

To estimate the occurrence more quantitatively, we note that *Kepler* observed only  $\sim 400$  stars with temperatures above about 9000 K (Batalha et al. 2010). Since the eclipse probabilities for systems like KOI 74 and KOI 81 are  $\sim 12\%$  and  $6\%$ , respectively, the detection of two such WD companions suggests that a surprisingly large fraction of such stars must have WD companions. With only two detections, it is difficult to estimate the orbital period distribution. Taking an average eclipse probability of  $\mathcal{P} \simeq 9\%$ , then for a fraction  $\mathcal{F}$  of A and B stars with suitably close WD companions, the mean number of expected eclipses among the *Kepler* sample would be  $\sim 400\mathcal{F}\mathcal{P}$ . The Poisson probability for finding two or more eclipses out of 400 systems is  $\sim 50\%$  for  $\mathcal{F} = 0.05$  and  $\sim 25\%$  for  $\mathcal{F} = 0.03$ . Therefore, we conclude that 1 out of every 20 to 30 A and B stars is in a close, few tens of days, binary with a WD companion.

The above abundance is very high, and, if confirmed, has significant implications for our understanding of stellar and binary evolution (see also Di Stefano 2010). For instance, the descendants of these systems should also be relatively numerous—and likely interesting—stars. When the currently more massive star leaves the main sequence and expands to overflow its Roche lobe, the resulting mass transfer will be dynamically unstable, and likely lead to a merger (even more likely than for Regulus, which has a longer period; see Rappaport et al. 2009). In this merger, the addition of a helium WD to the helium core of the subgiant star could lead directly to core helium ignition, bypassing the usual gradual buildup of the helium core via hydrogen shell burning. The merger product would also be rapidly rotating, and hence the natural outcome would appear to be a rapidly-rotating red clump or horizontal branch star (such as observed by, e.g., Behr et al. 2000 and Behr 2003).

Of course, while the above is interesting, it is possible that we are dealing with a statistical fluke. Indeed, if WD companions are very common among A stars, it seems odd that none has been reported so far for any of the much more numerous cooler stars in the *Kepler* sample. On the other hand, this may indicate that binary systems with initially lower-mass stars, which would evolve to G and F stars with low-mass WD companions, have a difficult time forming and/or surviving.

<sup>6</sup> In the binary calculation shown in Figure 2 (from the library of Podsiadlowski, Rappaport, & Pfahl 2002), the companion is a neutron star. The tracks for the KOI 74 and KOI 81 systems are expected to be very similar (see also Rappaport et al. 2009). For more details on the hydrogen shell flashes in these tracks, see Podsiadlowski et al. (2002) and Nelson, Dubeau, & MacCannell (2004).

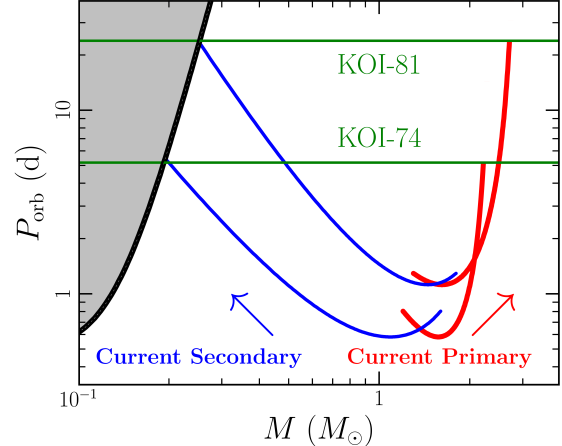


**Figure 3.** Example evolutionary histories in the mass-period plane. The red curves are for the mass-gaining stars, the blue curves for the mass-losing stars. The orbital periods of KOI 74 and KOI 81 are marked with green lines. The  $M_{\text{wd}}-P_{\text{orb}}$  relation, where the mass transfer terminates, is marked by a black curve. Many different such potential histories could be constructed.

Turning now to the formation of KOI 81 and KOI 74, for both the initial masses of the WD progenitors must have been greater than the initial masses of the current A stars, since the progenitors of the WDs have evolved more rapidly. Some form of binary interaction is needed in order to remove mass and produce the WDs. Either stable mass-transfer from the more massive to the less massive star has occurred; in this case, the current mass of the A star may be substantially higher than its initial mass (see, e.g., Rappaport et al. 2009). Alternatively, the system may have passed through a common-envelope phase (Paczynski 1976).

### 3.1. Stable Mass Transfer

If the mass loss from the progenitor of the WDs were simply through stable Roche-lobe overflow, then we could assume that the current orbital periods are very close to the orbital periods at the end of mass transfer, i.e., the point at which the mass of the envelope about each current WD became too small to maintain a giant structure and collapsed.<sup>7</sup> Hence we can apply the relationship between core mass and radius to predict the mass of each WD based on the current orbital periods. Using this relationship, Rappaport et al. (1995) approximated the orbital period  $P_{\text{orb}}$  as,

$$P_{\text{orb}} \approx 1.3 \times 10^5 \frac{M_{\text{wd}}^{6.25}}{(1 + 4M_{\text{wd}}^4)^{1.5}} \text{ days}, \quad (5)$$

where the WD mass  $M_{\text{wd}}$  is in units of solar masses. At a given  $P_{\text{orb}}$ , the spread in  $M_{\text{wd}}$  is expected to be at most  $\pm 15\%$ .

Applying Equation (5) we find  $M_{\text{wd}} = 0.20 \pm 0.03 M_{\odot}$  for KOI 74, which matches the value independently derived in Section 2. For KOI 81, this becomes  $M_{\text{wd}} = 0.25 \pm 0.03 M_{\odot}$ , again consistent with a low-mass WD.<sup>8</sup>

Stable mass transfer seems to provide a simple way to produce both these systems. The match between the WD masses from Equation (5) and from the light-curve data is encouraging. Furthermore, the full binary evolution calculations of

<sup>7</sup> A-type stars typically experience no magnetic braking, which might otherwise have shortened the orbital period since the end of mass-transfer.

<sup>8</sup> Tauris & Savonije (1999) provide an alternative expression, from which we obtain similar values:  $M_{\text{wd}} = 0.24 \pm 0.02 M_{\odot}$  for KOI 74 and  $M_{\text{wd}} = 0.29 \pm 0.02 M_{\odot}$  for KOI 81.

Podsiadlowski, Rappaport, & Pfahl (2002) produce systems with very similar orbital periods and WD masses (see their Fig. 13). In Figure 3, we show examples of how the two systems could have reached their current state, using simple analytic formulae for orbital evolution (Eq. (3) of Rappaport et al. 2009; see also Podsiadlowski, Joss, & Hsu 1992). The curves in Figure 3 take initial conditions  $\{M_{1,\text{init}}, M_{2,\text{init}}, P_{\text{orb,init}}\}$  of  $\{1.6M_{\odot}, 1.2M_{\odot}, 19.3\text{ h}\}$  for KOI 74 and  $\{1.8M_{\odot}, 1.3M_{\odot}, 31\text{ h}\}$  for KOI 81. In both cases we assume that any mass lost from the system carries away the specific orbital angular momentum of the binary. For KOI 74, this example assumes that the mass transfer is 73% conservative, and for KOI 81 it is 91% conservative. There are certainly other possible paths to the current systems, in particular since the above ignores the possible role of magnetic braking (in evolutionary stages where either star has a convective envelope).

The currently more massive stars are almost certain to have accreted significant amounts of matter and are therefore likely to be very rapidly rotating (see, e.g., Rappaport et al. (2009) and references therein). Their spin angular momentum could, in principle, have been lost by magnetic braking. However, typical A-type stars do not experience strong magnetic braking (see, e.g., Kawaler 1988). Alternatively, for KOI 74, tides might have been strong enough to slow the rotation of the star (and slightly widen the orbit).

### 3.2. Alternative: Common-envelope Evolution?

Common envelope evolution seems to provide a much less satisfactory explanation for these systems than stable mass transfer. If the envelopes of the initially more massive stars were ejected during common envelope evolution, then using the current  $P_{\text{orb}}$  in Equation (5) would only yield a minimum WD mass. So, if the observational data cannot allow more massive WDs than  $\sim 0.25M_{\odot}$ , it seems unlikely that either of these systems have experienced a significant common-envelope phase.

In addition, any scenario in which the currently more massive stars have *not* accreted a significant amount of mass seems difficult. The  $> 2M_{\odot}$  current primary stars in these systems would produce WDs more massive than  $\gtrsim 0.28M_{\odot}$  if their envelopes were removed at the end of the main sequence. If those initially less massive stars had not gained matter then, at best, significant fine-tuning would be required for the initially more massive star to have both evolved off the main sequence and produced the low-mass WDs observed.

### 3.3. Other Expected Compact Hot Companions: Hot Subdwarfs

Another class of hot compact companion stars that should result in light curves similar to those in Figure 1, are hot subdwarf (sdB, sdO) stars, sometimes referred to as extreme horizontal branch stars. The calculations of Han et al. (2002, 2003) predict that sdB stars should exist in binaries of these orbital periods about A- and B-type stars (see Han et al. 2003, Fig. 15). However, at the temperatures inferred for KOI 74 and 81, sdB stars would be expected to be considerably more luminous. Typical hot subdwarfs properties are anywhere between  $\sim 20000$  and  $40000\text{ K}$  and  $\sim 3$  and  $100L_{\odot}$ . In addition, the inferred companion masses in KOI 74 is somewhat too low to have ignited helium, even non-degenerately; masses greater than  $\sim 0.3M_{\odot}$  are required. Such hot subdwarfs should be found in current and future planetary transit searches.

## 4. SUMMARY

The wonderful photometric precision of *Kepler* has allowed us to measure the radial velocity amplitude of KOI 74. Combined with the primary mass inferred from its spectral type and mean density, we estimated a companion mass of  $0.22M_{\odot}$ , and argued it was a WD. We showed that its properties are in very good agreement with theoretical expectations based on a stable-mass transfer phase inside a binary system. A similar evolutionary history is also likely to have formed the current KOI 81 system. The many binaries that will be discovered by photometric surveys should be interesting and useful, both individually and collectively (see, e.g., Willems et al. 2006 for a quantitative study), in helping us to increase our understanding of binary evolution.

Future observations by *Kepler* should allow measurements of the photometric Doppler effect in more systems, perhaps including systems such as ‘ultra-cool white dwarfs,’ where the lack of spectral lines has precluded searches for radial velocity variations. Given long enough baselines, the photometric analog of the Rossiter-McLaughlin effect also seems likely to be observed.

Coffee-time astro-ph discussions at the Kavli Institute for Astronomy & Astrophysics triggered this work; in particular, we thank Yanqin Wu, Andrew Shannon & Matthias Gritschneider. We thank the referee, Scott Gaudi, for his careful reading and useful comments. S.A.R. and Ph.P. thank J. Rowe for sharing his work in advance of submission. S.J. thanks Bill Paxton for the plotting package Tioga.

*Facilities:* Kepler

*Note added in proof.* After acceptance of this article, high-resolution spectra were taken for us by E. Kirby using HIRES on the Keck I telescope. From these, we measure projected rotational velocities of 150 and 225 km/s for KOI 74 and KOI 81, respectively, and infer rotational periods of about 0.6 days for both sources. For KOI 74, the period is consistent with that inferred from the weak non-orbital modulation shown in the power spectrum (Section 2.2).

## REFERENCES

- Batalha, N. M. et al. 2010, *ApJ*, 713, L109  
 Beech, M. 1989, *Ap&SS*, 152, 329  
 Behr, B. B. 2003, *ApJS*, 149, 101  
 Behr, B. B., Djorgovski, S. G., Cohen, J. G., McCarthy, J. K., Côté, P., Piotto, G., & Zoccali, M. 2000, *ApJ*, 528, 849  
 Caldwell, D. A. et al. 2010, *ApJ*, 713, L92  
 Di Stefano, R. 2010, *ArXiv:1002.3009*  
 Gies, D. R. et al. 2008, *ApJ*, 682, L117  
 Han, Z., Podsiadlowski, P., Maxted, P. F. L., & Marsh, T. R. 2003, *MNRAS*, 341, 669  
 Han, Z., Podsiadlowski, P., Maxted, P. F. L., Marsh, T. R., & Ivanova, N. 2002, *MNRAS*, 336, 449  
 Hauschildt, P. H., Allard, F., & Baron, E. 1999, *ApJ*, 512, 377  
 Kawaler, S. D. 1988, *ApJ*, 333, 236  
 Koch, D. G. et al. 2010, *ApJ*, 713, L79  
 Loeb, A. & Gaudi, B. S. 2003, *ApJ*, 588, L117  
 Maxted, P. F. L., Marsh, T. R., & North, R. C. 2000, *MNRAS*, 317, L41  
 McAlister, H. A. et al. 2005, *ApJ*, 628, 439  
 McLaughlin, D. B. 1924, *ApJ*, 60, 22  
 Munari, U., Sordo, R., Castelli, F., & Zwitter, T. 2005, *A&A*, 442, 1127  
 Nelson, L. A., Dubeau, E., & MacCannell, K. A. 2004, *ApJ*, 616, 1124  
 Orosz, J. A. & Hauschildt, P. H. 2000, *A&A*, 364, 265  
 Paczynski, B. 1976, in *IAU Symposium, Vol. 73, Structure and Evolution of Close Binary Systems*, ed. P. Eggleton, S. Mitton, & J. Whelan, 75–+

- Panei, J. A., Althaus, L. G., Chen, X., & Han, Z. 2007, *MNRAS*, 382, 779
- Pfahl, E., Arras, P., & Paxton, B. 2008, *ApJ*, 679, 783
- Podsiadlowski, P., Joss, P. C., & Hsu, J. J. L. 1992, *ApJ*, 391, 246
- Podsiadlowski, P., Rappaport, S., & Pfahl, E. D. 2002, *ApJ*, 565, 1107
- Rappaport, S., Podsiadlowski, P., & Horev, I. 2009, *ApJ*, 698, 666
- Rappaport, S., Podsiadlowski, P., Joss, P. C., Di Stefano, R., & Han, Z. 1995, *MNRAS*, 273, 731
- Rossiter, R. A. 1924, *ApJ*, 60, 15
- Rowe, J. F. et al. 2010a, *ApJ*, 713, L150
- . 2010b, arXiv:1001.3420v1
- Russell, H. N. 1912, *ApJ*, 35, 315
- Stappers, B. W., van Kerkwijk, M. H., Lane, B., & Kulkarni, S. R. 1999, *ApJ*, 510, L45
- Tauris, T. M. & Savonije, G. J. 1999, *A&A*, 350, 928
- Willems, B., Kolb, U., & Justham, S. 2006, *MNRAS*, 367, 1103
- Zucker, S., Mazeh, T., & Alexander, T. 2007, *ApJ*, 670, 1326